

FLIR project - modeling noise in bolometer signal

Project group (alphabetic order):

Carl Ringqvist¹ carrin@kth.se

Giampaolo Mele¹ gmele@kth.se

Håkan Carlsson¹ hakcar@kth.se

Johan Karlsson¹ johan.karlsson@math.kth.se

Märta Barenthin Syberg² Marta.BarenthinSyberg@flir.se

Olof Runborg¹ olofr@nada.kth.se

Per Enqvist¹ penqvist@kth.se

Ulf Wällgren² ujpgwallgren@gmail.com

¹KTH

²FLIR

September 18, 2018

Abstract

A microbolometer is a device for measuring the power of incident electromagnetic radiation via the heating of a material with a temperature-dependent electrical resistance in infrared (IR) cameras. The change in the resistance is measured with an applied bias voltage, which yields a current that is fed to an integrator. The integrator then yields a readout voltage that represents the output signal of the system. The bias voltage also heats the resistance, and thus in the uncooled microbolometer system, the bias voltage is only applied periodically to allow the resistance to cool down. In the camera, an array of bolometers gives an IR image. Based on the heat equation and the Stefan Boltzmann law of black-body radiation, models can describe the underlying behavior of the bolometer, before the readout voltage. We would like to investigate if the underlying bolometer parameters can be identified using readout voltage data. Further, we investigate how noise affects the system and how the models can be modified to account for the noise. A better understanding of the components and the noise phenomena could potentially yield better detectors. This report is done in collaboration with FLIR, based in Täby. FLIR develops and produces cameras for temperature measurement.

Contents

1	Introduction	3
1.1	The IR camera	3
1.2	Project description	4
2	Model and discretization	5
2.1	Heat equation for the bolometer	5
2.2	Readout voltage equation	5
2.3	Illustrative example	6
2.4	Numerical methods for simulating the bolometer	7
3	Model with noise and discretization	9
3.1	Thermal noise	10
3.2	Flicker Noise	11
3.3	Noise model and simulation scheme	11
4	Numerical experiments	12
4.1	Solution with noisy model	12
4.2	Investigating model accuracy as function of σ	13
4.3	Noise dependence on integration time	15
4.4	Power spectrum of output signal	15
4.5	Linearity of the output signal	16
4.6	Spectrum of the output noise depending on spectrum of input noise	17
5	Outlook and future extensions	18
5.1	Noise process inclusion	18
6	Conclusion	19

1 Introduction

1.1 The IR camera

Electromagnetic radiation of wavelengths between 700 nanometer to 1 millimeter comprise what is usually referred to as *infrared light*. Much like the normal camera is able to detect and display variations of visible light (400 nanometers to 700 nanometers), infrared cameras produce pictures colored according to the variations in infrared radiation (IR) of a scene. Since infrared emission from an object is closely related to its temperature, an IR camera essentially produces a heat map to the eye, coloring parts of a scene relative to temperature. For instance in Figure 1, a cat is depicted based on the IR radiation it emits. Many infrared cameras are also able to accurately estimate the temperature of an object in addition to depicting it.

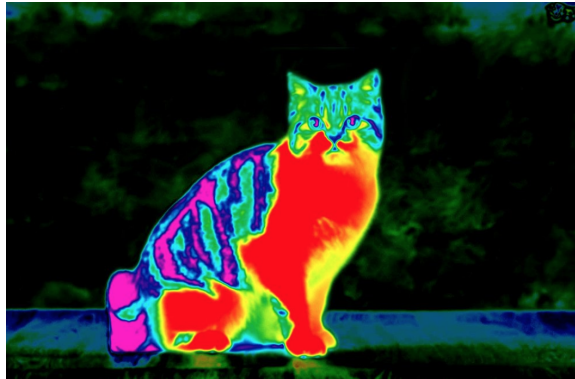


Figure 1: Infrared picture of a cat sitting on a table during night. The warmblooded cat is clearly distinguished from its cold surrounding, making the cat visible to the IR camera although not visible to the eye. Source: <https://www.scienceabc.com/>

Infrared cameras are used widely within industrial and military applications, enabling or enhancing tasks such as dark vision, heat leakage detection, moisture detection, chemical spill leakage detection and firefighting. An overview about different devices together with a catalog can be found in [1]. There exist mainly two types of techniques for infrared cameras: thermal detectors and quantum detectors. We will here focus solely on thermal detectors, and especially the *uncooled bolometer*. A bolometer consists of a plate (pixel) made of metal or semiconductor material, which for instance could be a mixture of silicon nitride and vanadium oxide. This plate is suspended in the air via two supporting legs that is connected to a substrate. The supporting legs are also connected to a voltage source. The structure is depicted in Figure 2. Incoming infrared radiation is focused via a lens to the plate, causing it to be heated, which in

turn alters its resistance. This change in resistance can be measured through an input voltage and the resulting current is a function of the strength of the incoming infrared radiation and hence the temperature of the emitting scene.

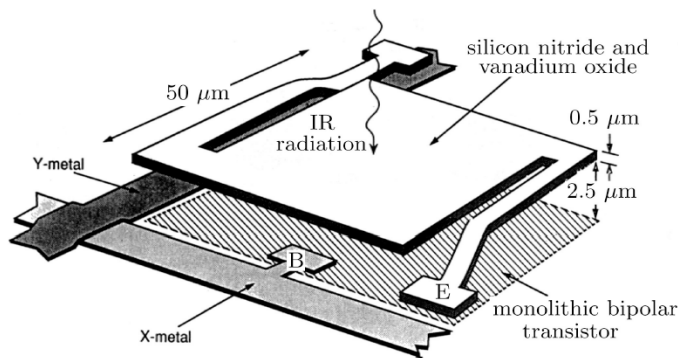


Figure 2: Physical structure of the bolometer [10].

1.2 Project description

The project aims to establish a mathematical relationship between the temperature of an object and the resulting bolometer signal. Briefly, the incoming radiation of an object, described by the Stefan-Boltzmann law, heats up the bolometer, which can be described by the heat equation. The applied voltage is used to measure the change in resistance due to the temperature change. More precisely, the output signal is a voltage from an integrator, that can be used to retrieve the change in the resistance and thus via the heat equation and the Stefan-Boltzmann law the temperature of the target. An explicit description of the output signal is given in Section 2.

In reality however, the output signal is noisy. The project aims to incorporate noise into the model in a manner consistent with data and experience. A good model of the noisy signal might for example enable applying an efficient filtering algorithm that reduces noise. The project's aim is to investigate how a noisy input signal affects the output signal.

More precisely in this project we:

- simulate the read-out signal of the bolometer by solving the differential equations modeling the problem,
- reproduce numerical simulations that fits with empirical experiments,
- model and analyze the noise in the differential equations,
- reproduce numerical simulations (with noise) that fits with empirical experiments.

2 Model and discretization

In this section, the heat equation for the bolometer and a model for the readout circuit are described.

2.1 Heat equation for the bolometer

The resistance $R(T)$ of the bolometer is a function of the temperature T , which for metals and semiconductors can be described by [10]

$$R(T) = R_s e^{\alpha(T-T_s)}, \quad (1)$$

where α is a constant that depends on the material of the bolometer, and R_s is the resistance of the bolometer at the substrate temperature T_s .

The temperature of the bolometer as a function of time (and the incoming IR radiation) can be described by the heat equation, the Stefan-Boltzmann law and the Joule heating law

$$C \frac{dT}{dt} = \frac{V_b(t)^2}{R(T)} + \varepsilon_e (P_t + P_s - 2A_s \sigma T^4) - G_{leg}(T - T_s), \quad (2)$$

$$T(0) = T_s.$$

Here $V_b(t)$ is the input voltage, ε_e is the material specific emissivity of the bolometer, P_t is the radiation power from the scene, P_s is the radiation power from the substrate, $2A_s$ is the total surface area of the bolometer (upside and downside), σ is the Boltzmann constant, and G is thermal conductivity of the supporting legs. The term $V_b(t)^2/R(T)$ is the power resulting from Joule heating, that is the power induced by the bias voltage over the bolometer, and $2A_s \sigma T^4$ represents the radiation power emitted from the bolometer according to Stefan-Boltzmann's law. The latter also relates P_t to the target temperature T_t of a scene object as $P_t \propto T_t^4$.

2.2 Readout voltage equation

Each pixel of an IR camera can be modeled as the circuit in Figure 3. More precisely the resistance of the bolometer corresponds to the resistor R2. To measure the resistance $R(T)$ a bias voltage is applied over the resistance R2. The bias voltage, however, excessively heats up the bolometer, and consequently the bias voltage is periodically shut off to let the bolometer cool down. This results in an input signal for the bias voltage that is a periodic square signal

$$V_b(t) = \begin{cases} v_b & nt_f < t < nt_f + t_i \\ 0 & \text{otherwise.} \end{cases} \quad n \in \mathbb{N} \quad (3)$$

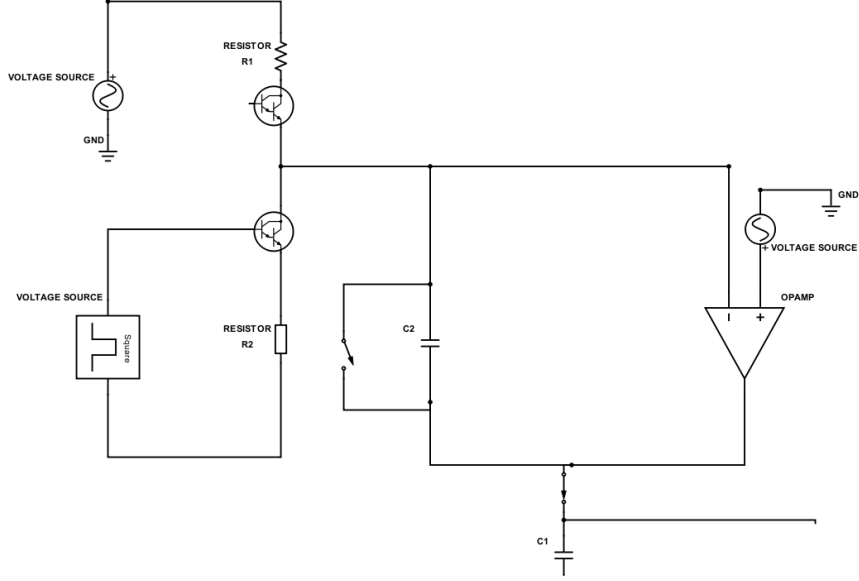


Figure 3: Circuit schematic that model a pixel of the IR camera generated with <https://www.digikey.com/schemeit>.

The resulting current from R2, is then subtracted from the current yielded from the resistance R1. This difference in current is then fed to the capacitor C2, which functions as an integrator. The voltage over the capacitor C2 is the readout voltage V_{samp} . Using Kirchoff's law, this voltage is expressed as

$$V_{samp} = \frac{1}{\tilde{C}} \int_{nt_f}^{nt_f+t_i} \left(\frac{V_0}{R_S} - \frac{V_b(s)}{R(T(s))} \right) ds + E \quad (4)$$

where \tilde{C} is the capacitance of C2. Clearly, in order to compute this integral, we need to know the temperature as function of the time. This relation is described by (2). Notice that V_{samp} does not depend on $R(T)$ if $V_b = 0$, and thus it is only relevant to integrate up to time t_i .

The output signal can therefore be simulated in the following way. We set an initial temperature T_0 for the bolometer and solve the heat balance equation (2). Then we compute the integral describing the readout signal (4).

2.3 Illustrative example

A reasonable and realistic simulation of the bolometer response can be obtained

Table 1: Parameters and coefficients used in Section 2.3

t_i	65	μsec	α	-0.02	
t_f	1/30	sec	e	0.8	
R_S	800	$k\Omega$	A	17	μm (square)
T_s	300	K	A_s	17	μm (square)
G_{leg}	250	μWK^{-1}	\tilde{C}	4	pF
C	25	nJK^{-1}	V_0	3.1	V
v_b	3	V	E	2	V

by solving the equations (2)-(4) with the parameters and coefficients given in Table 1. Moreover we have set $T_0 = T_s$, $P_t = A_s\sigma(T_0 + 10)^4$ and $P_s = A_s\sigma T_s^4$.

The solution of (2) is illustrated in Figure 4. In the phase when the bias voltage is active, usually referred as *integration time*, the temperature of the bolometer rises of circa $3K$. This is due to the fact that the current flowing through a component causes its overheat. When the bias voltage is not active, the temperature of the bolometer drops of circa $3K$, therefore we refer to this phase as *cooling time*. See Figure 5 for the illustration this such phenomena. The readout is illustrated in Figure 6.

As we can see in Figure 4-5, the temperature of the bolometer does not only depend on the incoming IR radiation, namely the temperature of the object we are observing, but also on the bias voltage. In order to mitigate this phenomena, the frame-time t_f is set much larger than the integration time t_i to avoid overheat the bolometer. In particular the function temperature T oscillates in the time (after very few pulses) around the temperature due to the incoming IR radiation. This also reflects in the readout, since V_{samp} becomes constant, i.e., the bolometer has cached the temperature of the observed object.

2.4 Numerical methods for simulating the bolometer

The output signal can be simulated by setting an initial temperature for the bolometer and by solving the heat balance equation (2). The readout V_{samp} corresponds to the integral (4) that can be approximated with any numerical integration algorithm such as Riemann sum, trapezoidal rule, etc. The equation (2) cannot be solved naively with a numerical scheme for ODE described, e.g., in [5, 2]. Namely, any `matlab` ODE solver is not capable of solving (2). This is due to the fact that the function $V_b(t)$ (bias voltage), defined in (3), has a very fast variation. The strategy for effectively solve the problem consists in splitting the domain in sub-domains where $V_b(t)$ is constant.

Assume that we want to solve (2) for $0 \leq t \leq mt$ for a fixed $m \in \mathbb{N}$, namely we

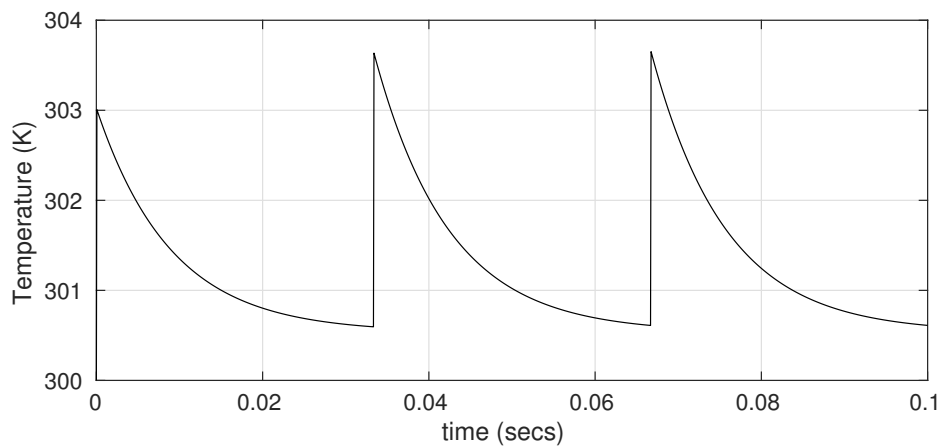


Figure 4: Solution to the heat balance equation (2).

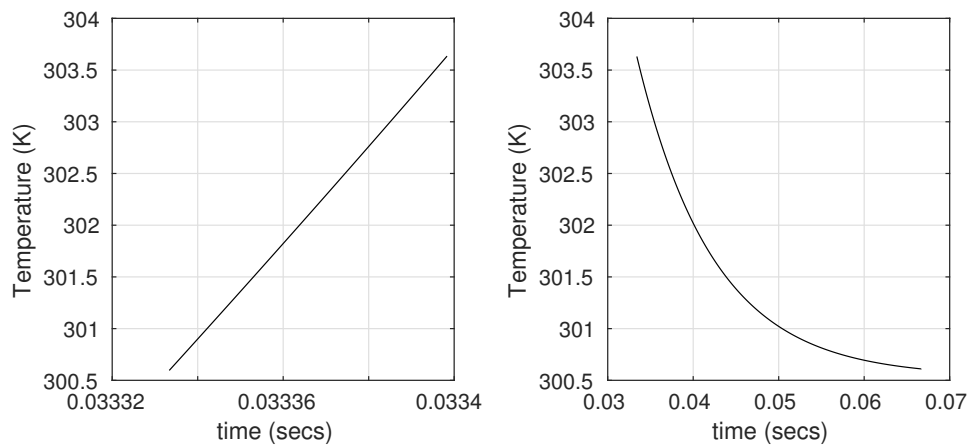


Figure 5: Solution to the heat balance equation (2) during the integration time $V_b > 0$, and during the cooling time $V_b = 0$.

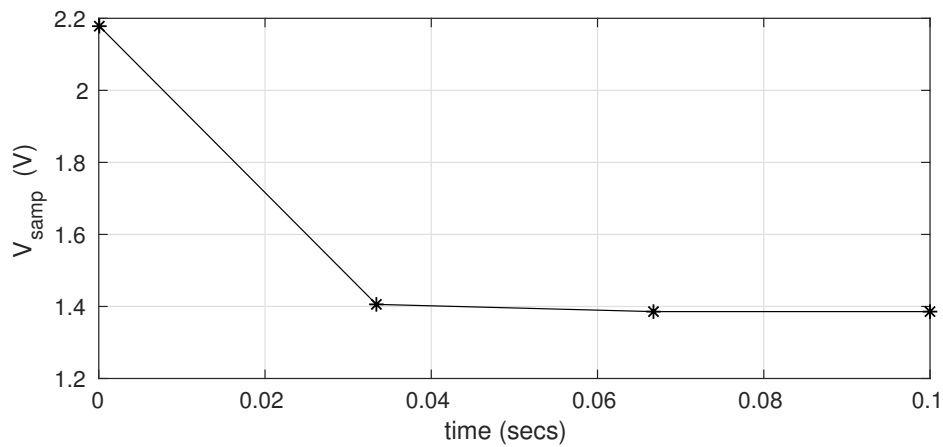


Figure 6: Readout voltage (4)

want m pulses. The time domain can be split as

$$[0, mt_f] = \bigcup_{k=0}^{m-1} (I_k \cup J_k)$$

where $I_k = [kt, kt_f + t_i]$ and $J_k = [kt_f + t_i, (k+1)t_f]$. We set $T_0(0) := T_0$ and for $k = 1, 2, \dots$, we solve the ODE in I_k

$$\begin{aligned} C \frac{dT_{k+1}}{dt} &= \frac{v_b^2}{R(T_{k+1})} + \epsilon_e(P_t + P_s - 2A\sigma T_{k+1}^4) - G_{leg}(T_{k+1} - T_s), \quad t \in I_k \\ T_{k+1}(kt_f) &= T_k(kt_f) \end{aligned} \quad (5)$$

we set $\alpha := T_{k+1}(kt_f + t_i)$ and we solve the ODE in J_k

$$\begin{aligned} C \frac{dT_{k+1}}{dt} &= \epsilon_e(P_t + P_s - 2A\sigma T_{k+1}^4) - G_{leg}(T_{k+1} - T_s), \quad t \in J_k \\ T_{k+1}(kt_f + t_i) &= \alpha_{k+1} \end{aligned} \quad (6)$$

The solution $T(t)$ of (2) is obtained by gluing the functions $T_j(t)$, i.e.,

$$T(t) = \begin{cases} T_0(t) & t \in I_0 \cup J_0 \\ T_1(t) & t \in I_1 \cup J_1 \\ \vdots & \\ T_k(t) & t \in I_k \cup J_k \\ \vdots & \\ T_m(t) & t \in I_m \cup J_m \end{cases}$$

In conclusion, the solutions of the ODEs (5)-(6) can be approximated with any numerical scheme such as Euler method, Runge-Kutta, etc. We did not observe any difficulty in solving these equations and we chose the explicit Euler method as solver since this can easily be extended to the noised model (stochastic differential equation) that we will introduce in the next section.

3 Model with noise and discretization

There are several sources of noise in a micro-bolometer setup:

- Thermal noise in the resistances,
- Flicker noise in resistances,
- Burst noise,
- Thermal fluctuations in the bolometer temperature,
- Noise in incident IR radiation,

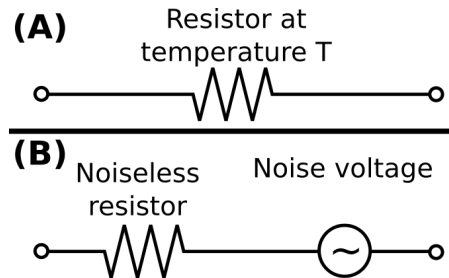


Figure 7: Equivalent model for thermal noise in a resistor.

- Noise in read out circuits.

In this report we shall only consider the first two types of noises, thermal and flicker noise in resistances.

3.1 Thermal noise

Any resistance with a temperature T above zero, will cause the charge carriers in the material to fluctuate. The fluctuations are independent of each other, and will generate a current with a voltage. This phenomenon is referred to as thermal noise, but is also known as white noise and Johnson noise. This type of noise was first discovered by the Swedish engineer John B. Johnson [3], and his colleague Harry Nyquist, also Swedish, provided a theory for the noise based on statistical physics[6]. One of the characteristics of the noise, is the flat power spectrum for all most all frequencies, which is also characteristic for white light.

In electrical circuits, thermal noise is commonly modeled as an additional power source in series with the resistance, see Figure 7. Due to the random nature of the additional power source, it is not possible to predict the instantaneous voltage produced, but instead the average behavior. Nyquist[6] found that the power spectrum of thermal noise to be

$$S(f) = 4k_B T R, \quad (7)$$

where k_B is the Boltzmann constant, T is the temperature of the resistance, and R is the resistance. The total contribution of the noise source is then calculated by summing up the contribution from each frequency component.

$$\mathbb{E}[V^2] = \int_B S(f) df, \quad (8)$$

where B is the bandwidth of the circuit.

A statistical model commonly used to white noise is a stationary stochastic

process where the auto-correlation function is

$$R(s, t) = \frac{\mathbb{E}[(X_t - \mu_t)(X_s - \mu_s)]}{\sigma_t \sigma_s} = \begin{cases} \sigma_t^2, & t = s, \\ 0, & t \neq s \end{cases} \quad (9)$$

meaning that the process is uncorrelated in time. A distribution that can be used for this process is the Gaussian distribution $\mathcal{N}(0, \sigma)$.

3.2 Flicker Noise

Another type of noise source that exists in circuits is flicker noise, or also known as low frequency noise, $1/f$ noise or pink noise. The power spectrum of the Flicker noise is

$$S(f) \propto \frac{k}{f^\alpha}, \quad (10)$$

where $\alpha \in [0.5, 1.5]$ and k is a material constant.

One explanation of the occurrence of the flicker noise in resistors is that the charge carriers get trapped in capture sites of the conductor, and are then released with variable rates. This was first explained by Schottky for flicker noise in vacuum tubes [7].

To generate the flicker noise in simulation there are several methods available, listed in [4] and [8].

3.3 Noise model and simulation scheme

To compensate for the noise in the read-out circuit, one first has to determine how noise enters the differential equation governing the behavior of the system. The simplest possible solution is of course to add a noise term of a normally distributed character to the left hand side in Equation (2), rendering the theory for diffusion processes readily available. More precisely we rewrite Equation (2) as

$$CdT = \left(\frac{V_b(t)^2}{R(T)} + \varepsilon(P_t + P_s - 2A_s \sigma T^4) - G_{leg}(T - T_s) \right) dt + K(t)dW \quad (11)$$

$$T(0) = T_s$$

where K is a function of time, and $W \sim N(0, dt)$. The function $K(t)$ is chosen according to the following heuristic. We expect the noise in the output to be the cause of resistor fluctuations. Motivated by the setup for Figure 7, we thus redefine the voltage over the bolometer resistance as

$$V \rightarrow V_0 + \Delta V, \quad (12)$$

where V_0 is the noise-less resistance over the voltage, and ΔV is a random variable representing the random fluctuations in the voltage.

We thus want noise to enter the heat equation in Equation (2) roughly as

$$C \frac{dT}{dt} = \frac{(V_b(t) + \Delta V)^2}{R(T)} + f(T), \quad (13)$$

where ΔV is the added noise term, accounting for the fluctuations in the resistance $R(T)$ and $f(T)$ are the other terms in Equation (2). Expanding the square we get the equation

$$C \frac{dT}{dt} = \frac{1}{R(T)} (V_b^2(t) + 2V_b(t)\Delta V + (\Delta V)^2) + f(T), \quad (14)$$

If the squared noise term is negligible in the limit, we are left with

$$C \frac{dT}{dt} = \frac{1}{R(T)} (V_b^2(t) + 2V_b(t)\Delta V) + f(T) \quad (15)$$

Thus we chose $K(t)$ in Equation (11) as $K(t) = 2V_b(t)\sigma$, where σ is a parameter to be calibrated or physically motivated. The noisy heat development can now be simulated in a well defined setting, with the dynamics independent of step size Δt :

$$CT_{i+1} = \left(\frac{V_b(t_i)^2}{R(T_i)} + \varepsilon(P_t + P_s - 2A_s\sigma T_i^4) - G_{leg}(T_i - T_s) \right) \Delta t + 2V_b(t_i)\sigma\sqrt{\Delta t}W_i \quad (16)$$

$$T(0) = T_s$$

where $W_i \sim N(0, 1)$.

4 Numerical experiments

In order to test that the model makes sense from a physical perspective, simulation experiments have been conducted. Expertise from FLIR has provided metrics against which outputs from the model has been benchmarked, along with suggestions for electronic design experiments. Below the resulting experiments are presented along with benchmarks if applicable.

4.1 Solution with noisy model

For the parameter σ , we set as a baseline

$$\sigma = \sqrt{4KT_sR(T_s)} \quad (17)$$

where K is the Boltzmann constant. This value is of order $1e^{-7}$ and is possible to motivate from a physical perspective. A detailed explanation can be found in [9].

We will however amplify or diminish σ depending on our needs with a constant d . Thus we will use

$$\sigma = d\sqrt{4KT_sR(T_s)} \quad (18)$$

Plots from running the temperature simulation and succeeding integrator with the noisy scheme outlined in Equation (16) are shown in Figure 8. We see that the difference from the deterministic solution is marginal, even with amplified noise.

4.2 Investigating model accuracy as function of σ

The model accuracy can be measured with the Noise Equivalent Temperature Difference (NETD), which has form

$$\text{NETD} = \frac{\text{std}(V(T, \sigma))}{V(T + 1, 0) - V(T, 0)} \quad (19)$$

It compares the standard deviation of the noisy output signal at temperature T with the difference in a deterministic signal when heating the observed object from T to $T + 1$. In other words, a large NETD indicates that the noise in the output is too large to detect a change of 1 degree in the observed object. Figure 9 depicts NETD over σ at $T = 300$. At this temperature, FLIR has estimated NETD to 20 mK. This knowledge lets us solve σ from the graph, resulting in a value of around $7e^{-6}$.

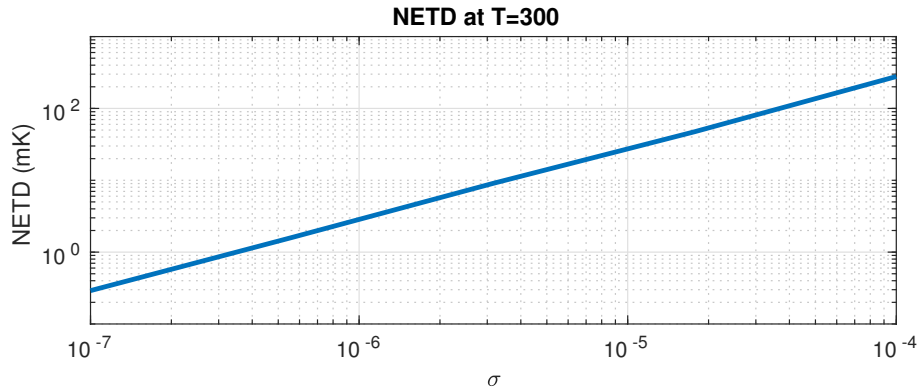


Figure 9: NETD as function of σ

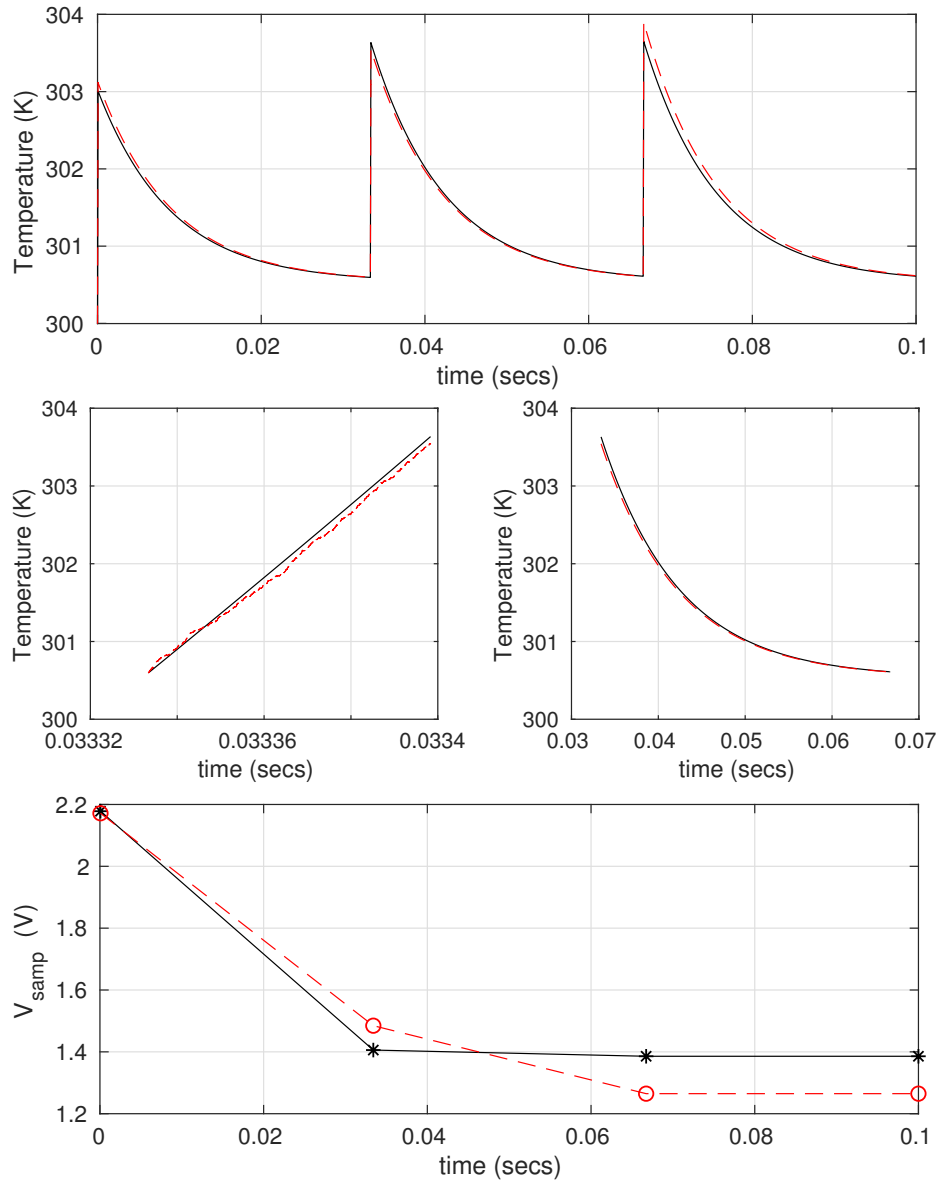


Figure 8: Temperature and output signal development over time for $d = 100$. Red: Noisy solution, Black: Deterministic solution

4.3 Noise dependence on integration time

Since measurements are collected only during integration time, a larger integration time on one hand acts to increase the measurement time-span and hence the reliability of the measurement. On the other hand, a larger integration time infers more substantial heating of the thermistor, resulting in increased noise. It is therefore of interest to investigate how the output noise depends on the integration time. In Figure 10, signal standard deviations for different frame rates are plotted against simulations of different integration times. The curve grows approximately as $t^{3/2}$. FLIR has estimated the curve to grow approximately as $t^{1/2}$, indicating our model is growing at too fast speed. This same peculiarity might explain that the plot of NETD over integration time is increasing, contrary to the experience at FLIR suggesting a decreasing NETD-curve.

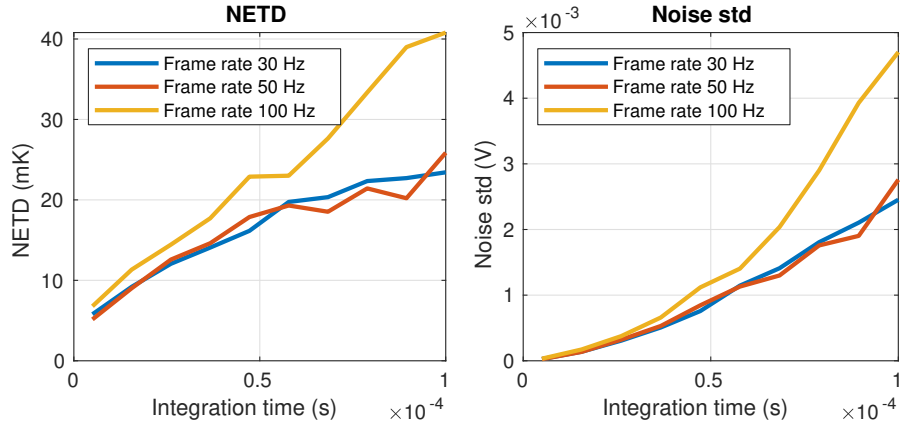


Figure 10: Output standard deviation over integration time

4.4 Power spectrum of output signal

Expertise from FLIR suggest that the power spectrum of the output signal is dependent on the frame-rate, and situated somewhere between the white and $1/f$ noise spectrum. In order to test the accordance between this experience and the model, the power spectrum of the output signal for different frame-rates have been generated. The result can be seen in Figure 11, together with a $1/f$ deterministic curve. Indeed, the output signal seems to shift from a white noise character to a $1/f$ character as frame-rates are altered.

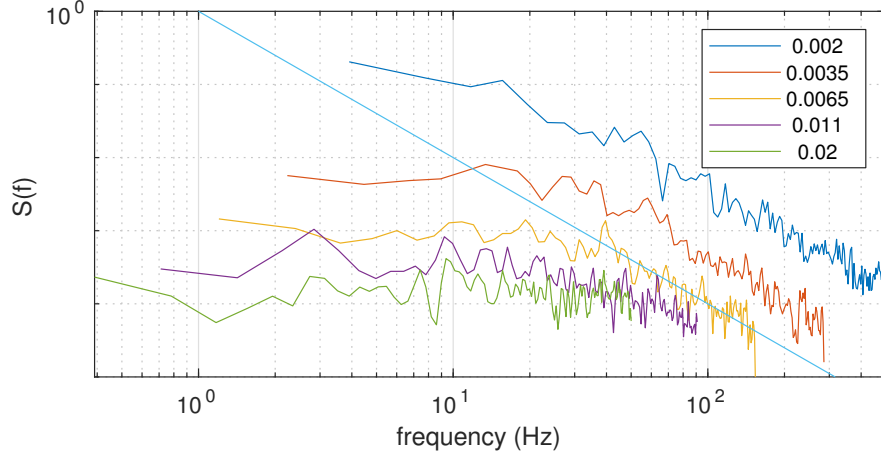


Figure 11: Power spectrum of output signal for different frame-rates $1/t_f$

4.5 Linearity of the output signal

The linearity of the output signal as a function of incoming radiation effect is an assumption made during the calibration process at FLIR. The deviation of the signal from this assumption require re-calibration of the camera at regular intervals. It is therefore of interest to investigate how this linearity is affected by factors possible to influence by design. For example, FLIR suggest that the design of the bias voltage curve during integration time might be important to achieve a higher degree of linearity in the output signal. In Figure 12, output signals V_{samp} over incoming effect P_t are plotted for different designs of bias voltage curve. The different bias voltage curves tested are

1. Constant voltage, as assumed in all previous simulations
2. Triangular voltage

$$V(t) = \begin{cases} ax + b & 0 \leq t \leq t_i/2 \\ cx + d & t_i/2 \leq t \leq t_i \end{cases}$$

3. Bell-curve

$$V(t) = \frac{1}{\sqrt{2\pi\sigma^2}} e^{-\frac{(x-\mu)^2}{2\sigma^2}} \quad 0 \leq t \leq t_i$$

4. Linear

$$V(t) = ax \quad 0 \leq t \leq t_i$$

All parameters in alternatives 1), 2), 3) are set to assure the power applied during integration time is the same as in the base case 1), and no noise is added

in this simulation. Interestingly enough, a tendency towards a more linear behavior is observed for the bell shaped bias voltage curve.

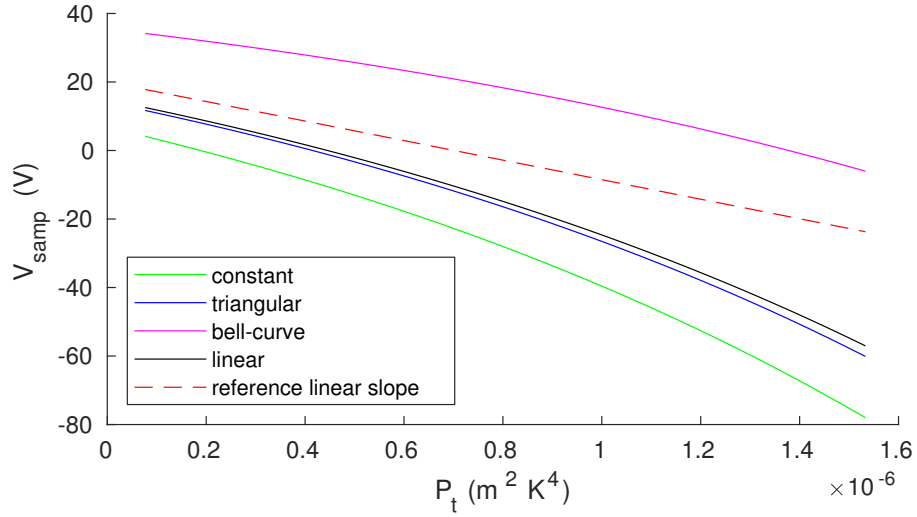


Figure 12: Power spectrum of output signal for different frame-rates

4.6 Spectrum of the output noise depending on spectrum of input noise

The noise of the voltage is suspected to contain a component with a $1/f$ spectrum, so called Flicker noise. It is therefore interesting to investigate the effect of replacing the noise term in Equation (11) with a term of $1/f$ spectrum. For a detailed explanation of how such a noise term is generated, see Section 3.2. The power spectrum of the output noise with $1/f$ noise as input is seen in Figure 13.

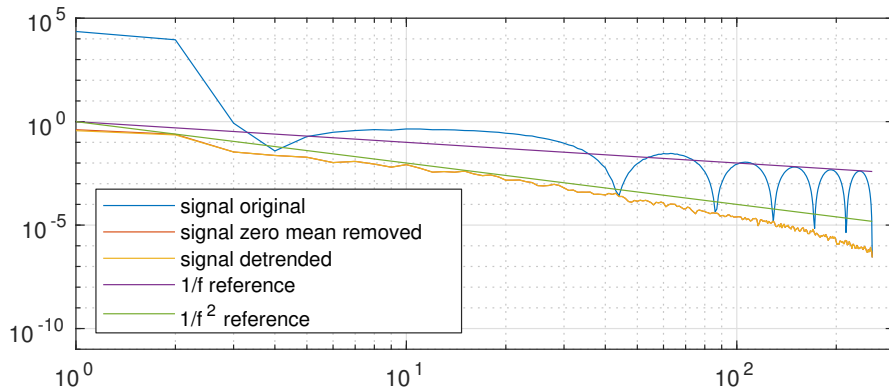


Figure 13: Power spectrum with $1/f$ noise in the input.

5 Outlook and future extensions

5.1 Noise process inclusion

In section 3 we went through the heuristic underlying the inclusion of noise in the model. This heuristic is however not entirely satisfactory. Although one can certainly argue for the negligibility of the squared noise term, it was dropped rather ad hoc. Neither did we account for the fact that the noise as inserted in the heuristics is subject to multiplication by a dt -term in the actual simulation, making it hard to establish a scaling scheme for the noise term with a well defined stochastic limit as step-size goes to 0. What we need in order to fully solve this matter is stochastic calculus.

Consider thermal noise and assume that the bias voltage $V(t)$ can be described as a diffusion process. Thermal noise has a white noise behavior, so ideally, stochasticity around the mean of the bias voltage $V_m(t)$ should have white noise form. Unfortunately, white noise is not possible to write as a diffusion process. We therefore suggest that $V(t)$ is modeled as follows:

$$dV = k(V_m(t) - V(t)) + \sigma dW_t$$

This is a Ornstein-Uhlenbeck process, which imposes a mean reverting mechanism. If the process is above $V_m(t)$, the drift term is negative and the process will tend to move towards $V_m(t)$. If the process is below $V_m(t)$, the reverse holds true. This makes correlation and variance increase over time limited when comparing to the standard Brownian e.g. By adjusting the constants σ and k , we can generate an erratic process dynamics with mean-adjusted noise much resembling white noise.

Let us consider what happens with the temperature dynamics in equation (2) when we assume the function $V(t)$ has the stochastic dynamics as described above. We are going to use the Lemma of Ito, which states that if a diffusion process X has dynamics $dX = \mu(t)dt + \sigma(t)dW_t$, then $f(X)$ (under certain regularity conditions) has dynamics

$$df = \left(\frac{\partial f}{\partial t} + \mu(t) \frac{\partial f}{\partial x} + \frac{\sigma(t)^2}{2} \frac{\partial^2 f}{\partial x^2} \right) dt + \sigma(t) \frac{\partial f}{\partial x} dW_t$$

In our case $f(x) = x^2$, so $\frac{\partial f}{\partial t} = 0$, $\frac{\partial f}{\partial x} = 2x$, $\frac{\partial^2 f}{\partial x^2} = 2$. Moreover, $\mu(t) = K(V_m(t) - V(t))$, and $\sigma(t) = \sigma$. Plugging in these values in the Ito formula gives

$$df = (k(V_m(t) - V(t))2V(t) + \sigma^2)dt + \sigma(t)2V(t)dW_t$$

or

$$dX(t) = (k(V_m(t) - \sqrt{X(t)})2\sqrt{X(t)} + \sigma^2)dt + \sigma(t)2\sqrt{X(t)}dW_t$$

Note that the temperature dynamics constitute a well defined stochastic process with the deterministic V replaced by the stochastic function X . The replacement operation turns the deterministic ODE into a diffusion process with another diffusion process (X) as drift coefficient. As X is adapted to the same underlying filter as T , the process is well defined via the Ito integral.

6 Conclusion

A mathematical model for the temperature evolution of a microbolometer and the corresponding output voltage was derived. The model is built using the heat equation, the Stefan Boltzmann's law, and the Joule heating law. The change in the temperature of the bolometer is measured through the resistance change. The heat equation model was modified based on heuristic arguments to include an additive noise term in the bias voltage, and the resulting differential equation was discretized and solved using the explicit Euler scheme.

This, however, led to counter intuitive results regarding the NETD and the power spectrum of the output voltage, raising the question whenever the assumed stochastic model was accurate enough. Unfortunately, there was no experimental data available to verify the numerical simulations to.

Nevertheless, hindsight provided us with a more well defined stochastic model to model the phenomena. Unfortunately, time was not enough to try out this idea.

References

- [1] The ultimate infrared handbook for r&d professionals. a resource guide for using infrared in the research and development industry. <http://www1.flir.com/science-guidebook>.
- [2] Uri M Ascher and Linda R Petzold. *Computer methods for ordinary differential equations and differential-algebraic equations*, volume 61. Siam, 1998.
- [3] J. B. Johnson. Thermal agitation of electricity in conductors. *Phys. Rev.*, 32:97–109, Jul 1928.
- [4] N. J. Kasdin. Discrete simulation of colored noise and stochastic processes and $1/f$ power law noise generation. *Proceedings of the IEEE*, 83(5):802–827, May 1995.
- [5] Robert Mattheij and Jaap Molenaar. *Ordinary differential equations in theory and practice*, volume 43. SIAM, 1996.
- [6] H. Nyquist. Thermal agitation of electric charge in conductors. *Phys. Rev.*, 32:110–113, Jul 1928.
- [7] W. Schottky. Small-shot effect and flicker effect. *Phys. Rev.*, 28:74–103, Jul 1926.
- [8] Miroslav Stoyanov, Max Gunzburger, and John Burkardt. Pink noise, $1/f^\alpha$ noise, and their effect on solutions of differential equations. *International Journal for Uncertainty Quantification*, 1(3):257–278, 2011.
- [9] R.A. Wood. Chapter 3 monolithic silicon microbolometer arrays. In Paul W. Kruse and David D. Skatrud, editors, *Uncooled Infrared Imaging Arrays and Systems*, volume 47 of *Semiconductors and Semimetals*, pages 43 – 121d. Elsevier, 1997.
- [10] Sui Xiu-Bao, Chen Qian, Gu Guo-Hua, and Liu Ning. Research on the response model of microbolometer. *Chinese Physics B*, 19(10):108702, 2010.